JBC RESEARCH ARTICLE

c-Src–mediated phosphorylation and activation of kinesin KIF1C promotes elongation of invadopodia in cancer cells

Received for publication, March 20, 2022, and in revised form, May 21, 2022 Published, Papers in Press, May 30, 2022,
https://doi.org/10.1016/j.jbc.2022.102090

Takeshi Saji[1,2], Michiru Nishita[1,2,*], Kazuho Ikeda[3], Mitsuharu Endo[2], Yasushi Okada[3,4,5,6], and Yasuhiro Minami[2,*]

From the [1]Department of Biochemistry, Fukushima Medical University School of Medicine, Fukushima, Japan; [2]Division of Cell Physiology, Department of Physiology and Cell Biology, Graduate School of Medicine, Kobe University, Kobe, Japan; [3]Department of Cell Biology, Graduate School of Medicine, The University of Tokyo, Tokyo, Japan; [4]Laboratory for Cell Polarity Regulation, RIKEN Center for Biosystems Dynamics Research (BDR), Osaka, Japan; [5]Department of Physics, Graduate School of Science, and [6]Universal Biology Institute (UBI) and International Research Center for Neurointelligence (WPI-IRCN), The University of Tokyo, Tokyo, Japan

Edited by Enrique De La Cruz

Invadopodia on cancer cells play crucial roles in tumor invasion and metastasis by degrading and remodeling the surrounding extracellular matrices and driving cell migration in complex 3D environments. Previous studies have indicated that microtubules (MTs) play a crucial role in elongation of invadopodia, but not their formation, probably by regulating delivery of membrane and secretory proteins within invadopodia. However, the identity of the responsible MT-based molecular motors and their regulation has been elusive. Here, we show that KIF1C, a member of kinesin-3 family, is localized to the tips of invadopodia and is required for their elongation and the invasion of cancer cells. We also found that c-Src phosphorylates tyrosine residues within the stalk domain of KIF1C, thereby enhancing its association with tyrosine phosphatase PTPD1, that in turn activates MT-binding ability of KIF1C, probably by relieving the autoinhibitory interaction between its motor and stalk domains. These findings shed new insights into how c-Src signaling is coupled to the MT-dependent dynamic nature of invadopodia and also advance our understanding of the mechanism of KIF1C activation through release of its autoinhibition.

Metastasis is a process by which primary cancers disseminate to secondary organs and is the main cause of mortality in cancer patients. The process includes key stages, such as cancer cell invasion, intravasation, and extravasation (1). Accumulating evidence demonstrates that finger-like structures on the surface of cancer cells, known as invadopodia, play a crucial role in degradation and remodeling of the surrounding extracellular matrices (ECMs) by recruiting various membrane and secretory proteins, such as integrins and matrix metalloproteinases (MMPs), thereby enabling cancer cells to migrate through the complex 3D microenvironments (2, 3). Invadopodia can also drive protease-independent cancer cell migration through confining 3D microenvironments, by mechanically opening up the channels and generating protrusive forces at the leading edge (4). Thus, structure and dynamics of invadopodia differ depending on the composition and mechanical properties of the microenvironments surrounding the cancer cells. Invadopodia consist of core F-actin bundles as well as proteins involved in actin dynamics, cell adhesion, membrane remodeling, and cell signaling (5–8). One of the cell signaling proteins that play pivotal roles in the formation and function of invadopodia is the nonreceptor type tyrosine kinase c-Src, which phosphorylates series of proteins localized to invadopodia, such as cortactin and Tks5, thereby recruiting other structural and functional proteins to invadopodia (9–12). Thus, the formation of invadopodia is promoted by ectopic expression of WT or constitutively active c-Src, while inhibited by ectopic expression of kinase-negative c-Src or siRNA-mediated knockdown of c-Src (13–15).

We have previously shown that signaling mediated by Ror2, a receptor for Wnt5a, promotes the formation of invadopodia in osteosarcoma cells in a c-Src–dependent manner (16). Comprehensive gene expression analysis has revealed that Ror2-mediated signaling induces expression of MMP-13 and intraflagellar transport 20 for promoting cancer invasion (16–18). During invasion, MMP-13 is targeted to invadopodia and induces focal degradation of ECM upon secretion (16). IFT20 is localized to the Golgi apparatus, where it promotes nucleation of Golgi-derived microtubules (MTs) for Golgi ribbon formation, thereby facilitating polarized transport of secretory and membrane proteins toward invadopodia (18). MT-based transport would thus be a critical step for invasive behavior of cancer cells. In fact, MTs have been shown to penetrate into long invadopodia, where membrane vesicles are observed along the MTs, and be essential for their elongation beyond 5 μm (8, 19). However, MT-based molecular motors that function within invadopodia remain to be identified.

KIF1C, a member of kinesin-3 family, would be a good candidate for the motor protein in the invadopodia, since it has been implicated in the formation of podosomes (20–22). Podosomes are invadopodia-like structures involved in degradation and remodeling of ECM, on the surface of normal

* For correspondence: authors: Michiru Nishita, nishita@fmu.ac.jp; Yasuhiro Minami, minami@kobe-u.ac.jp.

cells, such as macrophages and vascular smooth muscle cells. Invadopodia and podosomes contain similar, but not identical, molecular components, but their overall architectures are apparently different. In fact, invadopodia are highly protrusive and generated separately in an irregular pattern on the membrane, whereas podosomes are not protrusive and organized spatially into large assemblies as ring, belt, or rosette structures (23–25).

It is now widely appreciated that the transport activity of kinesin motors is generally regulated by the autoinhibition of kinesin and its release by the binding to cargoes or cargo-adapter proteins (26). Recent study has reported that KIF1C is autoinhibited by intramolecular interactions between its stalk and motor domains, which can be relieved upon binding of protein tyrosine phosphatase D1 (PTPD1) or the cargo-adapter protein Hook3 (27). Yet, another report (28) failed to reproduce it, possibly because the differences in the post-translational modification states of the KIF1C proteins between the two groups. Moreover, it is totally unclear whether and how KIF1C is regulated by c-Src, which is an essential kinase to promote the formation of invadopodia as described above.

Thus, previous studies on KIF1C have suggested its function in podosome formation, but its function in invadopodia has been elusive. Furthermore, the autoinhibition mechanism of KIF1C has been proposed as the regulatory mechanism, but its relation to c-Src has been totally unclear. Here, we uncover a novel function of KIF1C in invadopodia elongation, regulated by c-Src–mediated phosphorylation of KIF1C and its subsequent interaction with PTPD1

Results and discussion

KIF1C is dispensable for formation of short invadopodia but required for invasive migration

To elucidate the role of KIF1C in regulating invadopodia formation, we initially examined intracellular distribution of KIF1C in invasive human osteosarcoma SaOS2 cells. The cells were cultured on a thin layer of crosslinked gelatin labeled with Alexa Fluor 594 (Alexa-gelatin) or fluorescein (FL-gelatin), and invadopodia formation was assessed by monitoring dot-like accumulations of F-actin or cortactin, a prominent component of invadopodia, in the areas of degraded gelatin. KIF1C, fused to a fluorescent protein, was accumulated highly at the periphery of the cell, as reported previously (29) but failed to be localized to invadopodia (Fig. 1*A*). Similarly, KIF1C was not localized to invadopodia in highly invasive MDA-MB-231 breast cancer cells cultured on a thin layer of FL-gelatin (Fig. S1*A*). These results are in contrast to the observation that KIF1C was localized to podosomes generated on a thin layer of Alexa-gelatin in Src-transformed NIH3T3 cells (Fig. 1*B*). We also found that siRNAs against *KIF1C* failed to inhibit the formation of invadopodia on a thin layer of Alexa/FL-gelatin in SaOS2 and MDA-MB-231 cells (Fig. 1, *C* and *D*). These results clearly illustrate the difference between podosomes and invadopodia. KIF1C is reported to localize to podosomes in noncancer cells and is essential for their formation (20–22), while KIF1C is not required for the formation of invadopodia on a thin layer of gelatin. Notably, however, the same siRNAs significantly inhibited the invasive migration of SaOS2 and MDA-MB-231 cells through Matrigel-coated Transwell filters (Fig. 1*E*), indicating that KIF1C-depleted cells fail to invade through 3D matrices.

KIF1C is localized to the tips of invadopodia in 3D matrices and required for their elongation

To gain insight into how KIF1C regulates invasive migration, SaOS2 cells expressing KIF1C-Clover were cultured on a thick bed of Matrigel, which allows the cells to invade three-dimensionally, and distribution of KIF1C-Clover was examined. Confocal microscopic analysis revealed that KIF1C-Clover was localized to the tips of invadopodia, and these invadopodia contained MTs (Fig. 2*A*), indicating that KIF1C is localized to MT-containing invadopodia formed in 3D matrices. Unlike a thin layer of gelatin (2D matrices), 3D matrices allow spatial elongation of invadopodia, and MTs have been shown to be essential for their elongation (8, 19). Thus, our results suggest that KIF1C is activated at MT-containing invadopodia to facilitate their elongation in 3D matrices. The previous study used Matrigel-coated Transwell filters with 1 μm diameter to examine quantitatively the relationship between MTs and invadopodia length (8). By using the same assay system, we could detect invadopodia, recognized by phalloidin staining, in the filter pores, in SaOS2 and MDA-MB-231 cells, and these invadopodia were either positive or negative for KIF1C (Figs. 2*B* and S1*B*). KIF1C-positive invadopodia were also positive for an invadopodia marker, Tks5 (Figs. 2*C* and S1*C*). Cortactin and MTs were also present within the invadopodia in SaOS2 cells (Fig. 2, *D* and *E*). Quantification of the invadopodia length in the pores revealed that KIF1C-positive invadopodia were significantly longer than KIF1C-negative ones (Fig. 2*F*). Furthermore, length of invadopodia in the pores was significantly shortened in *KIF1C*-knockdown cells (Fig. 2*G*). From this length distribution, we noticed that more than 70% of invadopodia were longer than 5 μm in control cells, but the invadopodia in *KIF1C*-knockdown cells rarely exceed 5 μm (Fig. 2*G*). We, therefore, used this criterion for the following assays using SaOS2 cells. Namely, we classified cells into two types based on their short (<5 μm) and long (≥5 μm) average length of invadopodia. The proportion of cells with short and long average length of invadopodia serves as a compelling indicator for the effect of *KIF1C* knockdown (Fig. 2*H*). We also found that siRNAs against *KIF1C* reduce the length of invadopodia significantly in MDA-MB-231 cells (Fig. S1*D*). Thus, although cancer cells can generate short invadopodia through a KIF1C-independent mechanism, their subsequent elongation requires KIF1C. These results suggest that impaired elongation of invadopodia in *KIF1C*-depleted cells might be a cause of their reduced migratory activity through Matrigel-coated Transwell filters, shown in Figure 1*E*.

c-Src mediates tyrosine phosphorylation of KIF1C to promote its binding to PTPD1

It has previously been reported that KIF1C can be phosphorylated on tyrosine residue(s) when cells were treated with

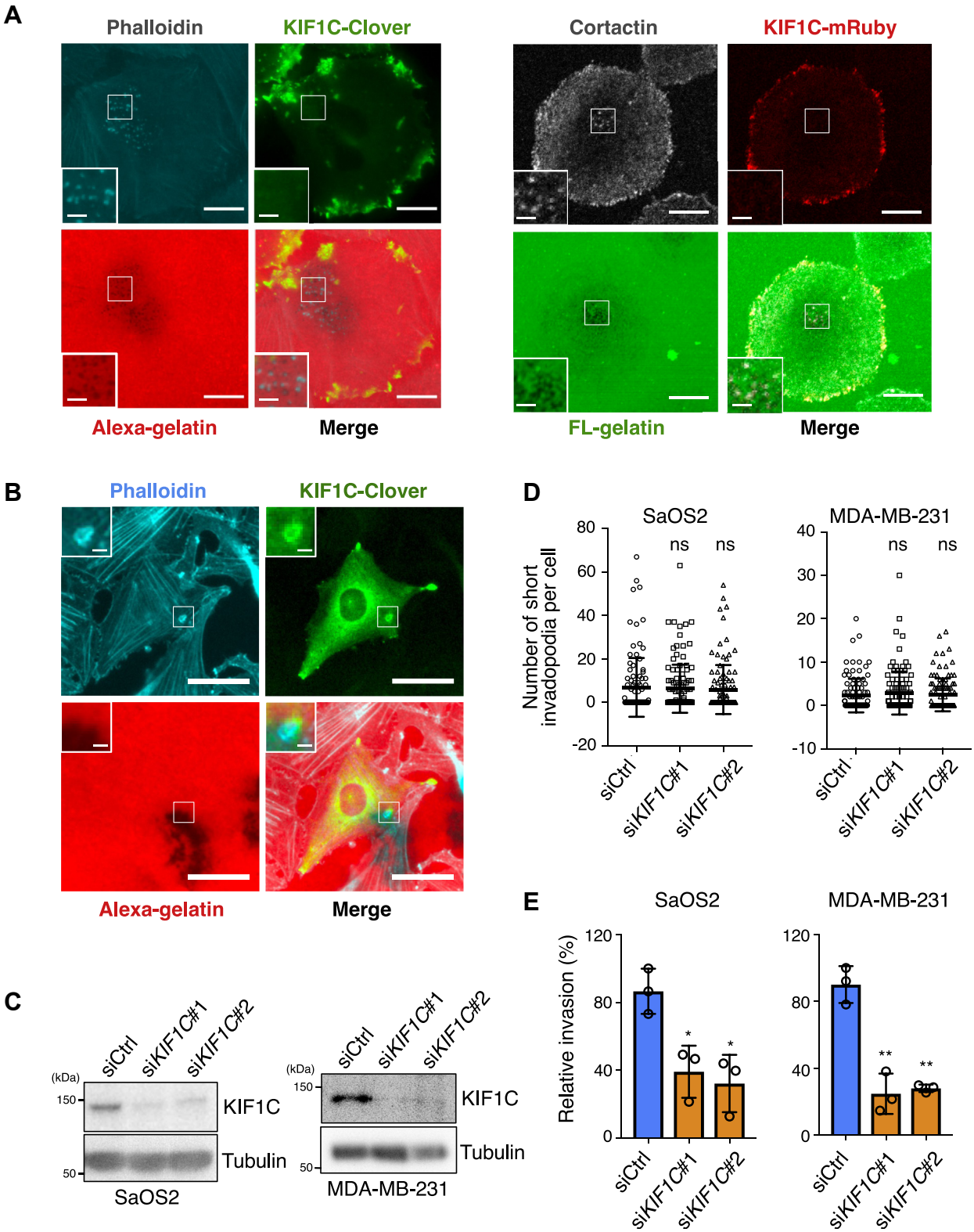

Figure 1. KIF1C is dispensable for the formation of short invadopodia but required for invasive cell migration. *A*, SaOS2 cells expressing KIF1C-Clover or KIF1C-mRuby were cultured on a thin layer of Alexa-gelatin or FL-gelatin and stained with phalloidin (F-actin) or anti-cortactin antibody as indicated. The scale bars represent 10 μm. *Insets* show magnified images of boxed regions (the scale bars represent 2 μm). *B*, Src-transformed NIH3T3 cells expressing KIF1C-Clover were cultured on a thin layer of Alexa-gelatin and stained with phalloidin. The scale bars represent 30 μm. *Insets* show magnified images of boxed regions (the scale bars represent 3 μm). *C*, immunoblot analysis showing decreased protein levels of KIF1C in SaOS2 and MDA-MB-231 cells transfected with si*KIF1C* (#1 or #2). *D*, SaOS2 or MDA-MB-231 cells transfected with the indicated siRNAs were cultured on a thin layer of FL-gelatin and stained with phalloidin. Number of invadopodia, identified as F-actin dots in the areas of degraded FL-gelatin, per cell was counted. Data are presented as mean ± SD. n = 101 to 107 (SaOS2) or 100 to 105 (MDA-MB-231) cells from three independent experiments; ns, not significant, Tukey test. *E*, SaOS2 or MDA-MB-231 cells transfected with the indicated siRNAs were analyzed by Transwell invasion assay. Cells invaded to the lower surface of the Transwell membranes were counted. Data are expressed as mean ± SD of three independent experiments, $*p < 0.05$, $**p < 0.01$, Tukey test. FL, fluorescein.

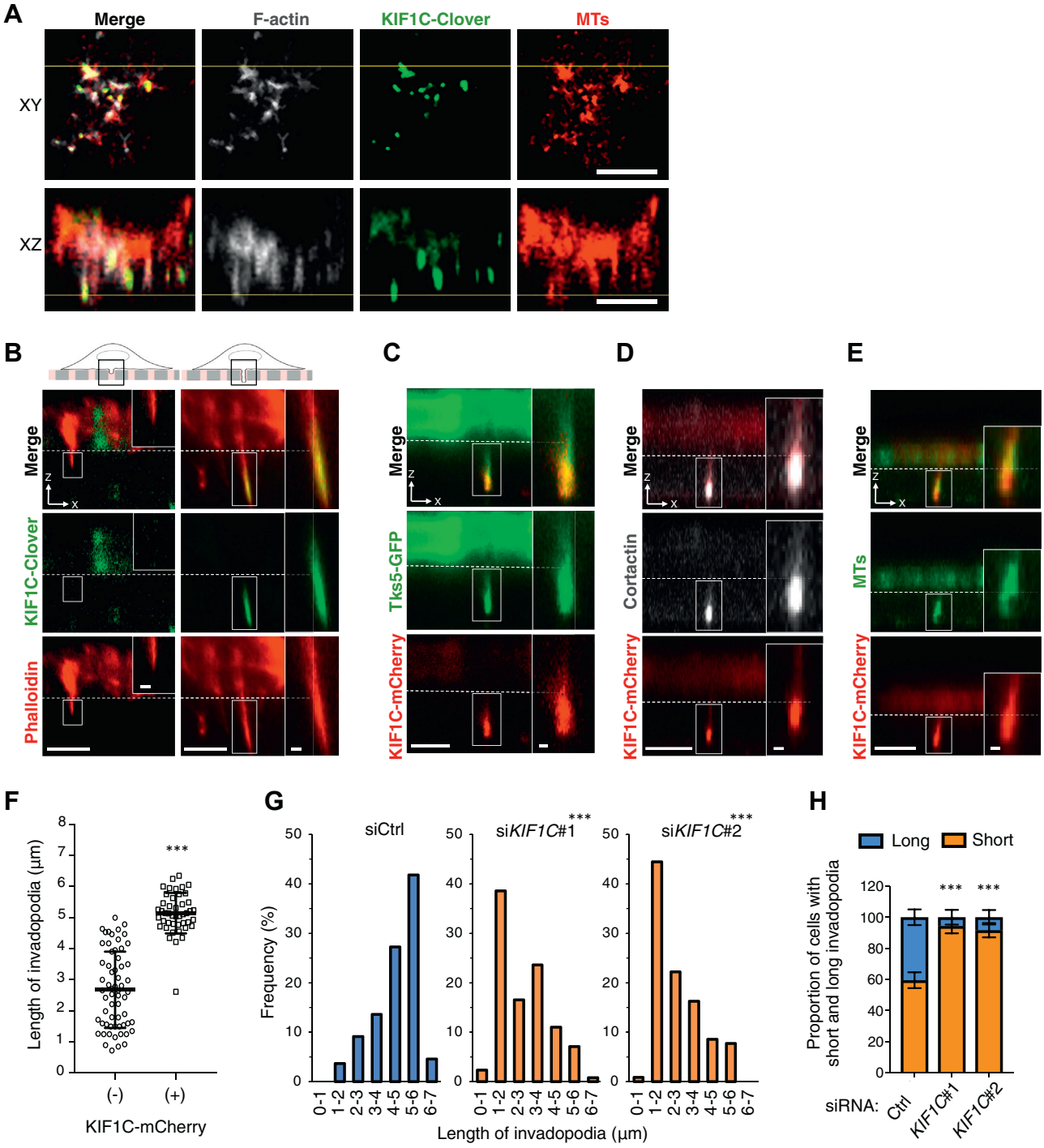

Figure 2. KIF1C is localized to the tips of invadopodia in 3D matrices and required for their elongation. *A*, SaOS2 cells expressing KIF1C-Clover were allowed to invade into a thick bed of FL-gelatin and stained with anti-tubulin (MTs) and phalloidin (F-actin). The xy and xz confocal images obtained along the respective *yellow lines* are shown. The scale bar represents 10 μm. *B*, SaOS2 cells expressing KIF1C-Clover were cultured on 1 μm diameter pore size. Transwell inserts precoated with Matrigel to induce formation of invadopodia through the pores, as illustrated in the schemes. Cells were stained with phalloidin. The xz images of cells extending KIF1C-Clover-negative (*left panels*) and positive (*right panels*) invadopodia are shown. *C–E*, SaOS2 cells expressing KIF1C-mCherry and Tks5-GFP (*C*) or KIF1C-mCherry alone (*D* and *E*) were cultured on the Transwell inserts as described in *B*. Cells were stained with anti-cortactin (*D*) or anti-α-tubulin (MTs) (*E*) antibody. The xz images of cells with KIF1C-mCherry-positive invadopodia are shown. *Dashed lines* indicate the upper surface of the filters. The scale bars represent 10 μm. Magnified images of boxed regions are shown on the *right* (the scale bars represent 1 μm). *F*, quantification of length of invadopodia. SaOS2 cells expressing KIF1C-mCherry were cultured on the Transwell inserts as described in (*B*) and stained with phalloidin. Length of invadopodia from 30 cells expressing KIF1C-mCherry were measured. Data are presented as mean ± SD. n = 45 and 62 (KIF1C-mCherry-positive and negative invadopodia, respectively), three independent experiments; ***$p < 0.001$, *t* test. *G*, length of invadopodia in SaOS2 cells transfected with the indicated siRNAs was quantified. The histograms indicate the frequency of invadopodia (% total invadopodia) with the indicated length. n = 110 (siCtrl), 132 (si*KIF1C#1*), and 117 (si*KIF1C#2*) invadopodia from 30 cells for each group, three independent experiments; ***$p < 0.001$, Steel test. *H*, proportion of cells with short (<5 μm) and long (≥5 μm) average length of invadopodia. Data are expressed as mean ± SD of three independent experiments, ***$p < 0.001$, Tukey test. FL, fluorescein; MT, microtubule.

peroxovanadate or KIF1C and c-Src were coexpressed in the cells (30), although phosphorylation site(s) on KIF1C and its biological relevance remain to be defined. Accumulating evidence supports the notion that c-Src is an important component of invadopodia and plays a key role in the formation and function of invadopodia by phosphorylating other components, including cortactin, Tks5, and p130CAS (24, 31). Thus, we hypothesized that c-Src might phosphorylate KIF1C to mediate robust elongation of invadopodia in cancer cells. Confocal laser microscopic and coimmunoprecipitation analyses revealed that KIF1C and c-Src are colocalized to invadopodia and interact physically each other, respectively (Fig. 3, *A* and *B*). The levels of KIF1C coprecipitated with constitutively active form of c-Src (Y527F) were lower than those coprecipitated with WT c-Src (Fig. 3*B*), presumably reflecting faster association/dissociation rates of c-Src-Y527F with KIF1C. Consistently, anti-phosphotyrosine immunoblotting of immunoprecipitated KIF1C showed that KIF1C was tyrosine phosphorylated more heavily by c-Src-Y527F than by c-Src-WT (Fig. 3*C*). By generating a series of truncated mutants of KIF1C, we found that the C-terminal half of the motor domain (amino acids 176–350) was necessary for binding between KIF1C and c-Src (Fig. S2).

We have previously shown that Wnt5a-Ror2 signaling induces activation of c-Src and thereby promotes the formation of invadopodia and invasive migration of osteosarcoma cells (16). We therefore examined the effect of Wnt5a stimulation on the levels of phospho-tyrosine on KIF1C in SaOS2 cells. We found that Wnt5a treatment induced tyrosine phosphorylation of endogenous KIF1C, which could be inhibited by the presence of dasatinib, a potent inhibitor of the Src-family kinases (Fig. 3*D*), indicating that Wnt5a/c-Src signaling induces phosphorylation of KIF1C in SaOS2 cells. We then sought to identify tyrosine residue(s) within KIF1C that are phosphorylated by c-Src. Since 11 tyrosine residues were predicted to be potential phosphorylation sites within KIF1C by using the NetPhos 3.1 server (http://www.cbs.dtu.dk/services/NetPhos/) (32), we substituted these tyrosine residues individually with phenylalanine and assessed whether the respective YF substituted mutant proteins exhibit reduced tyrosine phosphorylation when coexpressed with c-Src-Y527F. We found that, among the 11 KIF1C mutants, four YF mutants (Y654F/Y671F/Y726F/Y757F) exhibited reduced tyrosine phosphorylation levels compared with those of KIF1C-WT (Fig. S3), indicating that these four tyrosine residues are candidate phosphorylation sites by c-Src. We then generated KIF1C-4YF mutant, in which all of the four tyrosine residues are substituted with phenylalanine and confirmed considerably reduced tyrosine phosphorylation of KIF1C-4YF by c-Src-Y527F (Fig. 3*E*).

It is now widely appreciated that the transport activity of kinesin motors is generally regulated by the autoinhibition of kinesin and its release by the binding to cargoes or cargo-adapter proteins (26). Recent study has reported that KIF1C is autoinhibited by intramolecular interactions between its stalk and motor domains, which can be relieved upon binding of PTPD1 or the cargo-adapter protein Hook3 (27). Notably, four tyrosine residues identified as candidate phosphorylation sites within KIF1C (Y654, Y671, Y726, Y757) were found within the region involved in its binding to PTPD1 (27), raising a possibility that c-Src–mediated phosphorylation of KIF1C regulates its binding to PTPD1. To test this possibility, we examined the effect of c-Src (WT or Y527F) expressed ectopically on binding between KIF1C and PTPD1 by coimmunoprecipitation assay. We used the FERM domain of PTPD1 ($PTPD1_{FERM}$) since it is sufficient to interact with and activate KIF1C (27). We found that binding between KIF1C and $PTPD1_{FERM}$ was enhanced moderately by c-Src-WT, and more drastically by c-Src-Y527F, consistent with their effects on KIF1C phosphorylation (Fig. 3*F*). Furthermore, the amount of $PTPD1_{FERM}$ coprecipitated with KIF1C-4YF was substantially lower than that coprecipitated with KIF1C-WT in the presence of c-Src-Y527F (Fig. 3*G*). Essentially, similar results were obtained when full length PTPD1 was expressed instead of $PTPD1_{FERM}$ (Fig. 3*H*). Together, these results indicate that c-Src induces phosphorylation of KIF1C within its stalk domain to enhance its binding to $PTPD1_{FERM}$.

c-Src–mediated tyrosine phosphorylation of KIF1C is required for elongation of invadopodia and invasive cell migration

To further assess the biological relevance of c-Src–mediated phosphorylation of KIF1C during cancer cell invasion, we performed rescue experiments using siRNA-resistant *KIF1C* constructs. We found that ectopic expression of sr*KIF1C-WT*, but not sr*KIF1C-4YF*, could rescue the effects of *KIF1C* siRNA on the proportion of short and long invadopodia (Fig. 4*A*), as well as on invasive cell migration (Fig. 4*B*), suggesting that c-Src–mediated phosphorylation of the four tyrosine residues (Y654, Y671, Y726, Y757) within KIF1C is required for transition from short to robust long invadopodia and invasive cancer cell migration. Interestingly, in control siRNA-transfected cells, ectopic expression of sr*KIF1C-4YF* resulted in increased and decreased proportion of short and long invadopodia, respectively (Fig. 4*A*), as well as reduced invasive cell migration (Fig. 4*B*), similar to the effect of *KIF1C* siRNA. Since KIF1C can form a stable dimer that is autoinhibited by intramolecular interactions and is activated by $PTPD1_{FERM}$ binding (27), KIF1C-4YF is likely to act as a dominant negative mutant by dimerizing with endogenous KIF1C.

To gain further insight into the dominant negative function of KIF1C-4YF, we examined whether ectopic expression of KIF1C-4YF can interfere with peripheral localization of KIF1C-WT that depends on its motor activity (27). To this end, KIF1C-WT-mCherry was coexpressed with either KIF1C-WT-Clover or KIF1C-4YF-Clover in SaOS2 cells. Although the fluorescence signal of KIF1C-WT-mCherry overlapped largely, if not completely, with that of either KIF1C-WT-Clover or KIF1C-4YF-Clover, the latter showed reduced peripheral accumulation and instead increased cytoplasmic distribution (Fig. 4*C*). In fact, the ratio of peripheral *versus* cytoplasmic KIF1C-WT-mCherry intensity was significantly lower in cells coexpressing KIF1C-4YF-Clover than that in cells coexpressing either KIF1C-WT-Clover or GFP (Fig. 4*C*).

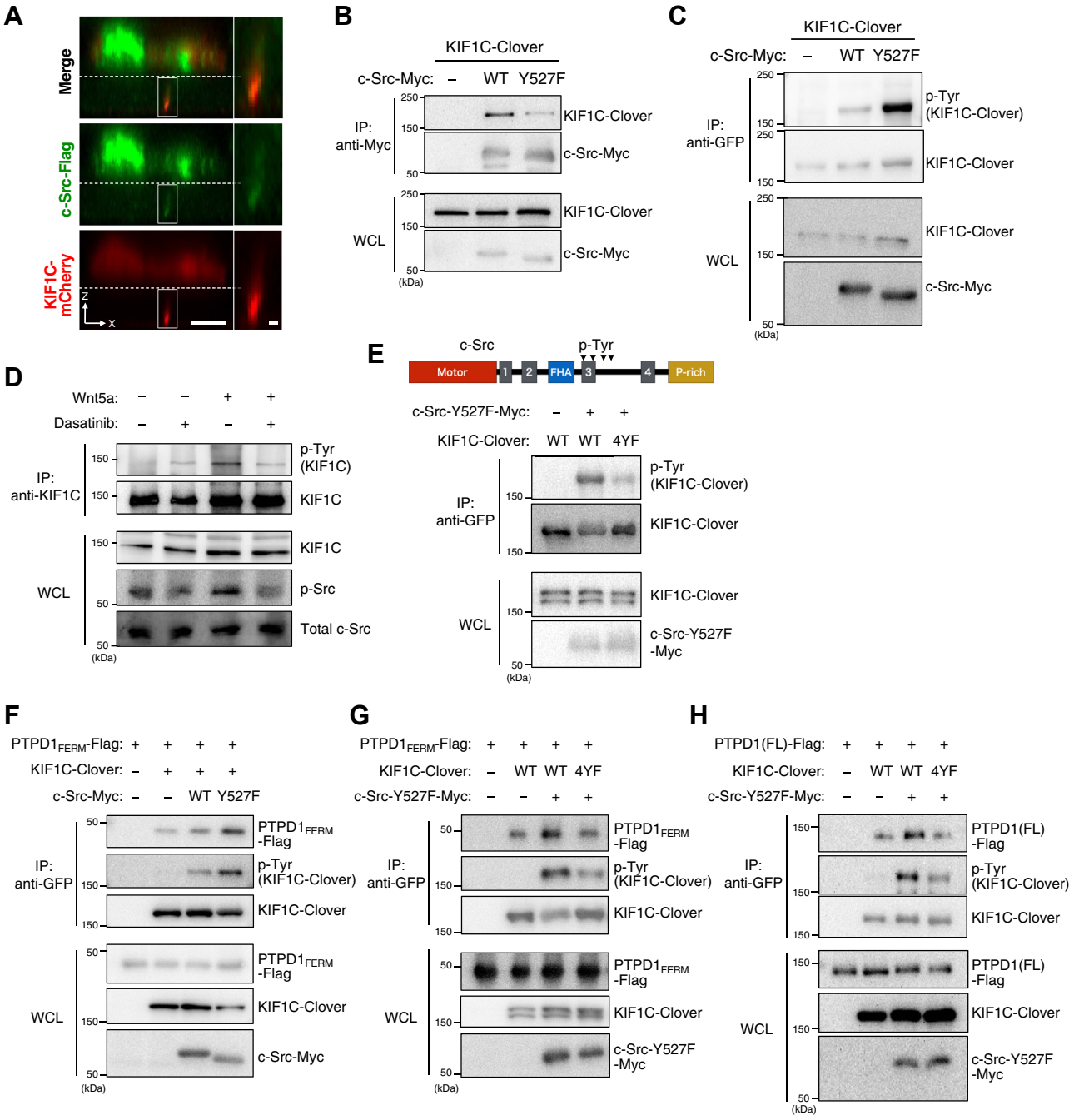

Figure 3. c-Src induces phosphorylation of KIF1C to enhance its binding to PTPD1. *A*, SaOS2 cells expressing KIF1C-mCherry and c-Src-Flag were cultured on the Transwell inserts as described in Figure 2*B* and stained with anti-Flag antibody. The xz images of the cell with KIF1C-mCherry-positive invadopodia are shown. *Dashed lines* indicate the upper surface of the filters. The scale bar represents 10 μm. Magnified images of boxed regions are shown on the *right* (The scale bar represents 1 μm). *B*, association of KIF1C with c-Src. HEK293T cells were cotransfected with KIF1C-Clover and c-Src (WT or Y527F)-Myc. Whole cell lysate (WCL) or anti-Myc immunoprecipitates were analyzed by immunoblotting. *C*, tyrosine-phosphorylation of KIF1C by c-Src. HEK293T cells were cotransfected with KIF1C-Clover and c-Src (WT or Y527F). WCL or anti-GFP immunoprecipitates were analyzed by immunoblotting. *D*, Wnt5a stimulation enhances c-Src–mediated phosphorylation of KIF1C. Serum-starved SaOS2 cells were treated with Wnt5a (final conc. of 400 ng/ml) for 1 h in the presence or absence of 10 nM Dasatinib. WCL or anti-KIF1C immunoprecipitates were analyzed by immunoblotting. *E*, *top*, schematic primary structure of KIF1C with motor, forkhead-associated (FHA), proline-rich (P-rich), and coiled-coil (*gray boxes* 1–4) domains. c-Src–binding region (c-Src) and four tyrosine residues phosphorylated by c-Src (p-Tyr), identified in this study, are indicated. *Bottom*, HEK293T cells were cotransfected with KIF1C (WT or 4YF)-Clover and c-Src-Y527F-Myc. WCL or anti-GFP immunoprecipitates were analyzed by immunoblotting. *F*, association of KIF1C with $PTPD1_{FERM}$ is promoted by c-Src. HEK293T cells were cotransfected with $PTPD1_{FERM}$-Flag, KIF1C-WT-Clover, and c-Src-Myc (WT or Y527F). WCL or anti-GFP immunoprecipitates were analyzed by immunoblotting. *G* and *H*, c-Src fails to promote association of KIF1C-4YF with PTPD1. HEK293T cells were transfected with $PTPD1_{FERM}$-Flag (*G*) or PTPD1(FL: full length)-Flag (*H*) together with KIF1C (WT or 4YF)-Clover and c-Src-Y527F-Myc. WCL or anti-GFP immunoprecipitates were analyzed by immunoblotting. PTPD1, protein tyrosine phosphatase D1.

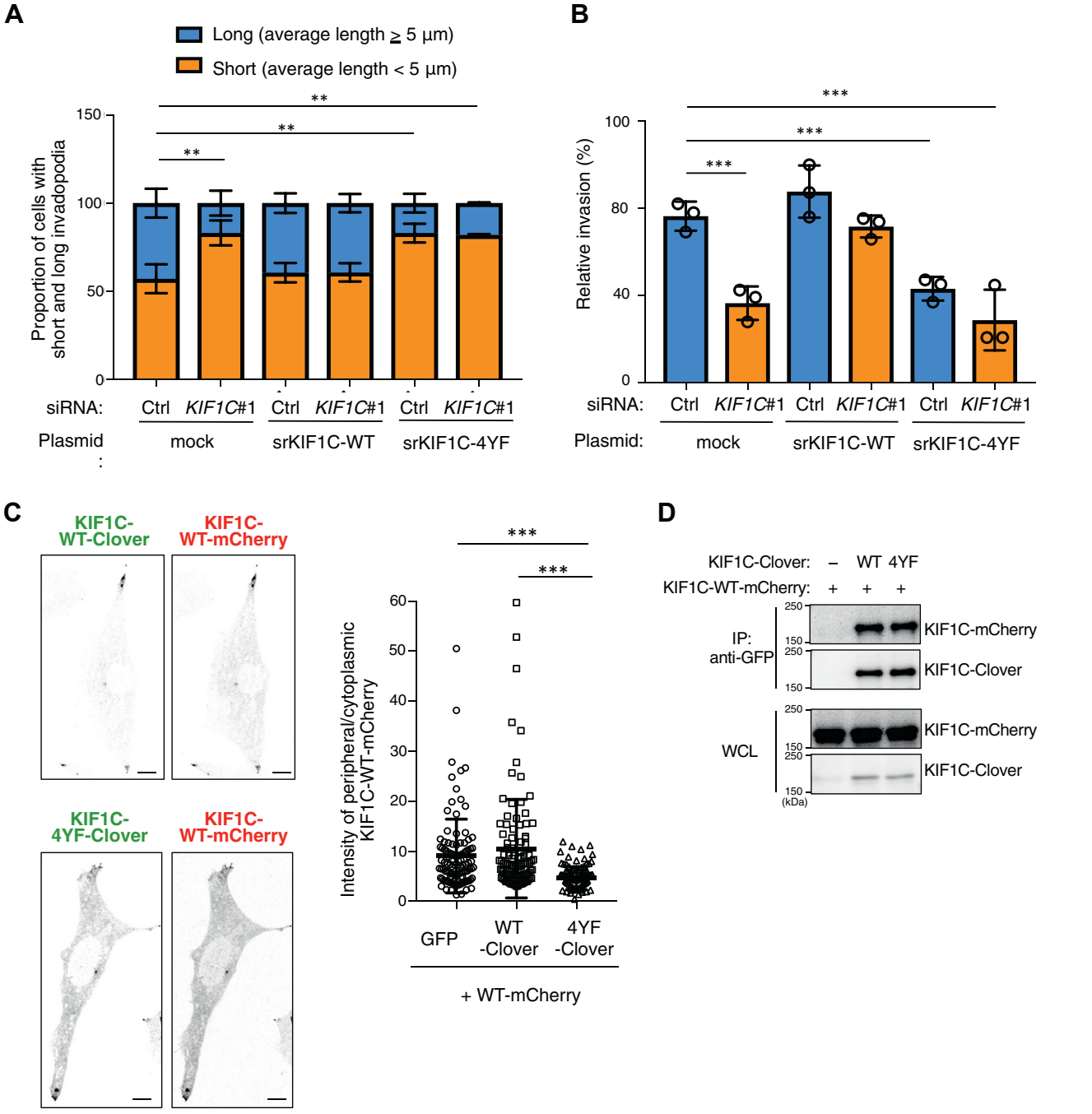

Figure 4. c-Src–mediated phosphorylation of KIF1C is required for elongation of invadopodia and invasion. *A*, SaOS2 cells transfected with siCtrl or si*KIF1C#1* were further transfected with sr*KIF1C* (WT or 4YF)-Clover that is resistant to si*KIF1C#1*. Cells were cultured on the Transwell inserts and stained with phalloidin as described in Figure 2*B*, and proportion of cells with short (<5 μm) and long (≥5 μm) average length of invadopodia was quantified. Data are expressed as mean ± SD of three independent experiments, $^{**}p < 0.01$, Tukey test. *B*, U2OS cells stably expressing GFP (mock), srKIF1C-WT-Clover, or srKIF1C-4YF-Clover were transfected with siCtrl or si*KIF1C*#1 and analyzed by Transwell invasion assay. Data are expressed as mean ± SD of three independent experiments, $^{***}p < 0.001$, Tukey test. *C*, *left*, representative inverted *gray* scale images of SaOS2 cells coexpressing KIF1C-WT-mCherry and either KIF1C-WT-Clover (*top panels*) or KIF1C-4YF-Clover (*bottom panels*). The scale bars represent 10 μm. *Right*, intensities of mCherry fluorescence at the peripheral/nonperipheral cytoplasmic regions of cells were quantified. Cells coexpressing KIF1C-WT-mCherry and GFP were also used as a control. Data are presented as mean ± SD. n = 102 to 109 from 30 cells, three independent experiments, $^{***}p < 0.001$, Steel test. *D*, SaOS2 cells were cotransfected with KIF1C-WT-mCherry and either KIF1C-WT-Clover or KIF1C-4YF-Clover. WCL or anti-GFP immunoprecipitates were analyzed by immunoblotting.

Furthermore, both KIF1C-WT-Clover and KIF1C-4YF-Clover bound comparably to KIF1C-WT-mCherry as assessed by coimmunoprecipitation assay (Fig. 4*D*), indicating that KIF1C-4YF is indeed a dominant negative mutant with reduced motor activities, thereby inhibiting elongation of invadopodia and invasive cancer cell migration.

c-Src–mediated tyrosine phosphorylation of KIF1C is required for its binding to MTs

Previous studies have shown that an autoinhibition of some KIFs, including KIF1C, through their intramolecular interaction, prevents their motor domain from interacting with MTs (27, 33–35). To gain further insight into how c-Src–mediated

phosphorylation of KIF1C affects its motor activity, we examined the MT binding abilities of KIF1C-WT or KIF1C-4YF in cells. To this end, SaOS2 cells expressing KIF1C-Clover (WT or 4YF) with or without c-Src-Y527F-Myc were treated with cold methanol, in which proteins were extracted and fixed concurrently and stained with antibodies against α-tubulin and Myc-tag. We found that substantial proportion of KIF1C-WT-Clover, but not its 4YF mutant, was colocalized with MTs when coexpressed with c-Src-Y527F (Fig. 5*A*). Quantification revealed that colocalization between KIF1C-WT and MTs is significantly increased by ectopic expression of c-Src-Y527F, and this colocalization is greater than colocalization between KIF1C-4YF and MTs in the presence of c-Src-Y527F. Consistent with these findings, MT cosedimentation assay revealed that binding of KIF1C-WT-Clover, but not KIF1C-4YF-Clover, with MTs was augmented obviously when coexpressed with c-Src-Y527F (Fig. 5*B*). These results suggest that c-Src–mediated phosphorylation of KIF1C potentiates its binding to MTs by relieving autoinhibition.

In conclusion, we show for the first time that KIF1C is localized to long invadopodia, but not short ones, in cancer cells, that is consistent with MT localization in long, but not short invadopodia. As previously reported, MTs are not essential for the generation of short invadopodia, which are sufficient to degrade a thin layer of ECM (8, 19). In fact, most of the studies on invadopodia thus far have focused on short ones generated on a thin layer of matrix. However, such experimental conditions appear to be distinct from actual 3D environments, where invading cancer cells often need to extend long invadopodia to drive cell migration through confined spaces (2, 8, 36). KIF1C might move along MTs within invadopodia to deliver membrane lipids and proteins required for their elongation to their tips.

We also clarified the regulatory mechanism for KIF1C activity, especially the role of c-Src–mediated phosphorylation within its stalk domain, where PTPD1 can bind to relieve autoinhibition of KIF1C in a phosphatase activity–independent manner (27). Interestingly, PTPD1 has been shown to interact with and dephosphorylate Tyr527 residue of c-Src, leading to its activation (37, 38). Thus, PTPD1 recruited to c-Src–phosphorylated KIF1C might contribute to drive a positive feedback loop that promotes c-Src–mediated phosphorylation and activation of KIF1C within invadopodia to ensure their continuous elongation. Beside PTPD1, the cargo-adapter protein Hook3 has been shown to interact with the stalk domain of KIF1C (27, 28). Although one group observed that, like PTPD1, Hook3 increased landing rate of KIF1C onto MTs, another group failed to reproduce it. Since KIF1C proteins used by the two groups were from different sources, there might be differences in the tyrosine phosphorylation states within the stalk domain of the KIF1C proteins between the two groups, leading to their controversial results.

Experimental procedures

Plasmids and siRNAs

Human *KIF1C* cDNA clone (IRAK047K20) was provided by the RIKEN BRC and subcloned into pEGFP-N1-based vectors, pClover-N1, pmRuby-N1, and pmCherry-N1, in which the sequence for EGFP was replaced by the sequence for Clover, mRuby, and mCherry, respectively. To construct an expression plasmid encoding KIF1C-Clover resistant to si-*KIF1C*#1 (sr*KIF1C-Clover*), six bases in the 19-base target sequence in the corresponding *KIF1C* cDNA were altered by PCR amplification (GTGTCTTACATGGAAATTT). Expression plasmids encoding the series of truncated KIF1C-Clover were constructed by subcloning cDNAs encoding the following *KIF1C* fragments into the pClover-N1 vector, respectively: Δ175 (aa 175–1103), Δ350 (aa 350–1103), Δ1 (aa 1–900), Δ2 (aa 1–810), Δ3 (aa 1–700), Δ4 (aa 1–600), Δ5 (aa 1–500). The following point mutations were introduced into sr*KIF1C-Clover* by site-directed mutagenesis: Y516F, Y569F, Y654F, Y671F, Y726F, Y757, Y786, Y1061F, Y1068F, Y1078F, Y1081F, and 4YF (Y654F/Y671F/Y726F/Y757F). To construct retroviral vectors encoding KIF1C-WT-Clover and KIF1C-4YF-Clover, the corresponding cDNAs were inserted into pLPCX vector (Clontech). To construct expression plasmids encoding Flag-tagged full length human PTPD1 (PTPD1-Flag) and its FERM domain ($PTPD1_{FERM}$-Flag), the corresponding cDNAs were amplified from 293T cells and inserted into pcDNA-Flag vector. Expression plasmids for c-Src-Myc and its Y527F mutant in pCX4 vector (39) were kindly provided by M. Okada. To construct plasmid encoding c-Src-Flag, cDNA encoding c-Src was subcloned into pcDNA3-Flag vector. Expression plasmids for human Tks5 in pEGFP vector (40) was provided by T. Oikawa. The sequences of the siRNAs used were as follows: si-*KIF1C*#1, 5′-(GUGAGCUAUAUGGAGAUCUdTdT)-3′; and si-*KIF1C*#2, 5′-(CCCAUGCCGUCUUUACCAUdTdT)-3′ (Sigma). MISSION siRNA Universal Negative Control #1 (si-Ctrl) was purchased from Sigma.

Cell culture, transfection, and retroviral infection

SaOS2, U2OS, MDA-MB-231, and 293T cells were cultured in Dulbecco's Modified Eagle's Medium (DMEM) (FUJIFILM Wako Pure Chemical Corporation) containing 10% (v/v) fetal bovine serum (FBS). Src-transformed NIH3T3 cells (expressing Y530F mutant of human c-Src) (41) were kindly provided by T. Itoh and cultured in DMEM containing 10% (v/v) FBS. For siRNA transfection, RNAiMAX (Thermo Fisher Scientific) was used according to the manufacturers' instructions. For plasmid transfection, Viafect (Promega) and Lipofectamine 2000 (Thermo Fisher Scientific) were used for SaOS2, MDA-MB-231, and 293T cells, respectively. For retroviral infection, 293T cells were transfected with pLPCX-*KIF1C-Clover* (WT or 4YF) plasmid together with pE-ampho and pGP plasmids (Takara). After 48 h, viral supernatant was collected and filtered through a 0.45 μm diameter pore size membrane. U2OS cells were infected with the viral supernatant in the presence of 10 μg/ml polybrene for 24 h. Subsequently, infected cells were selected in the growth medium containing 1 μg/ml puromycin for 1 week, and then puromycin-resistant cells were collected for analysis.

Antibodies and reagents

Following antibodies were obtained commercially: anti-KIF1C (BETHYL), anti-p-Src-Y416 (Cell Signaling

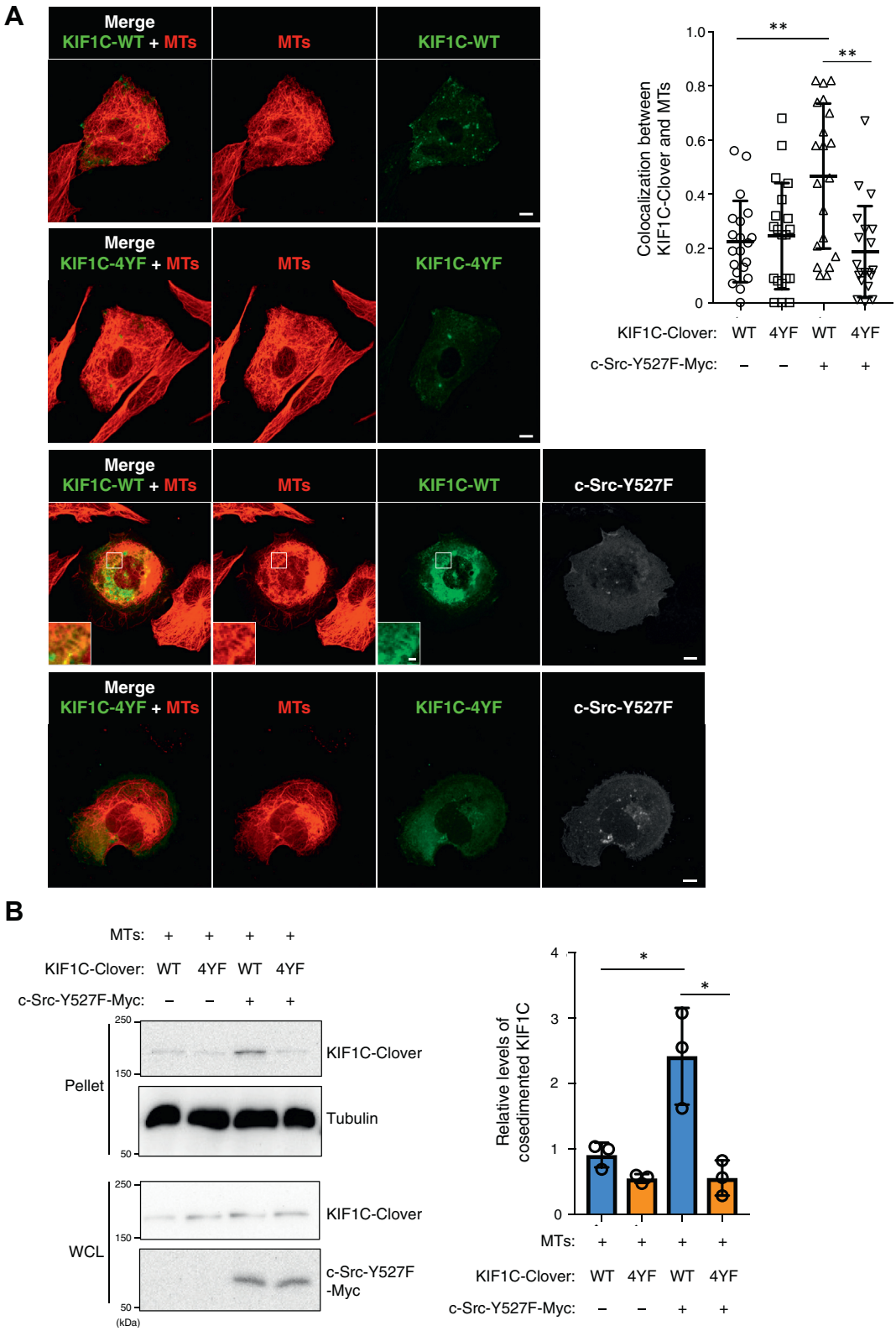

Figure 5. c-Src–mediated phosphorylation of KIF1C is required for its binding to MTs. *A*, *left*, SaOS2 cells expressing KIF1C (WT or 4YF)-Clover with or without c-Src-Y527F-Myc were fixed with methanol and immunostained with anti-α-tubulin (MTs) and anti-Myc antibodies. Representative images are shown. The scale bars represent 10 μm. *Insets* show magnified images of boxed regions (the scale bar represents 1 μm). *Right*, colocalization between KIF1C-Clover and MTs was quantified. Data are presented as mean ± SD. n = 20 cells from three independent experiments; $^{**}p < 0.01$, Tukey test). *B*, *left*, SaOS2 cells were cotransfected with KIF1C (WT or 4YF)-Clover and c-Src-Y527F-Myc, lysed, and mixed with stabilized MTs. KIF1C-Clover cosedimented with MTs were analyzed by immunoblotting. *Right*, the relative levels of cosedimented KIF1C were calculated by the band intensity on immunoblots. Data are expressed as mean ± SD of three independent experiments, $^{*}p < 0.05$, Tukey test. MT, microtubule.

Technology), anti-c-Src (CALBIOCHEM), anti-Flag (M2), anti-Myc for IP (9E10, Santa Cruz) and WB (A14, Santa Cruz), anti-α-tubulin (MBL), anti-GFP (that recognizes Clover) for immunoprecipitation (Sigma) and immunoblotting (JL-8, Takara), anti-RFP (that recognizes mCherry) (MBL), anti-cortactin (4F11, Millipore), and anti-Phosphotyrosine (4G10, Millipore). Dasatinib was purchased from Cell Signaling Technology.

Immunoprecipitation and immunoblotting

Cells were lysed in ice-cold lysis buffer (50 mM Tris–HCl, pH7.4, 0.5% (v/v) Nonidet P-40, 150 mM NaCl, 5 mM EDTA, 50 mM NaF, 1 mM Na_3VO_4, 1 mM *p*-PMSF, 10 μg/ml leupeptin, and 10 μg/ml aprotinin). The resultant lysates were subjected to immunoprecipitation, SDS-PAGE, and immunoblotting as described previously (42).

Alexa-gelatin degradation assay

Coverslips or glass bottom dishes were coated with a thin layer of Alexa- or FL-conjugated gelatin and crosslinked with 0.5% glutaraldehyde, as previously described (18). Cells were seeded on these coverslips or glass bottom dishes and then incubated for 6 h at 37 °C. Cells were washed with PBS and fixed with 4% (w/v) paraformaldehyde. Cells were permeabilized with 0.2% (v/v) TritonX-100 in PBS and then blocked with 5% (w/v) BSA in PBS. Blocked cells were stained with the respective antibodies and phalloidin conjugated with Alexa Fluor-488, Alexa Fluor 647, or rhodamine (Invitrogen). Fluorescence images were obtained using a LSM700 with Plan-Apochromat 40×/1.4 NA and 63×/1.4 NA oil immersion objective lenses (Carl Zeiss).

Imaging analyses of invasion in Matrigel

Coverslips were coated with undiluted Matrigel (Corning) with a thickness of at least 100 μm, which we term thick bet of Matrigel. Cells transfected with expression plasmids and siRNAs were seeded on these coverslips and then incubated for 2 h at 37 °C. Cells were fixed with 4% (w/v) paraformaldehyde, permeabilized with 0.2% (v/v) TritonX-100, and then blocked with 5% (w/v) bovine serum albumin (BSA) in PBS. Blocked cells were stained with anti-α-Tubulin antibody and phalloidin. Fluorescence images were obtained with an A1 confocal microscope (Nikon). ImageJ software (National Institutes of Health) was used for Z-stack projection.

Imaging analyses of invadopodia formation through filter pores

Transwell inserts with a 10.5-mm-diameter, 1 μm diameter pore size membrane (Corning) were coated with 40 μl Matrigel (1:20 in DMEM) for 1 h at 4 °C, 30 μl Matrigel was removed, and then Transwell chamber was incubated for 1 h at 37 °C. 1.5×10^4 cells transfected with siRNAs or plasmids in serum-free DMEM were loaded to upper well. The lower well was filled with DMEM containing 10% (v/v) FBS. After incubation for 15 h at 37 °C, cells were washed with PBS and fixed with 4% (w/v) paraformaldehyde. After cells were stained with antibody or phalloidin, serial optical sections were obtained with a confocal microscope LSM700 (Carl Zeiss) or A1, and length of invadopodia was measured from the xz projections of the image stack using ImageJ software.

Transwell invasion assay

Transwell invasion assay was performed as described previously (16). In brief, Transwell inserts with a 10.5-mm-diameter, 8 μm diameter pore size membrane (Corning) were coated with Matrigel (1:20 in DMEM) for 1 h at 37 °C. 2.5×10^4 cells transfected with siRNAs or plasmids in serum-free DMEM were loaded onto the upper well. The lower well was filled with DMEM containing 10% FBS. After incubation for 12 h, cells invaded to lower surface of the membrane were counted.

In vivo *MT-binding assay*

SaOS2 cells were plated onto coverslips coated with fibronectin and then transfected with plasmids. After incubation for 24 h, cells were washed with PBS and treated with cold (−20 °C) methanol for 15 min to extract and fix proteins concurrently. After washing three times with PBS, cells were blocked with 5% (w/v) BSA in PBS and stained with antibodies against α-tubulin and Myc tag. Fluorescence images were obtained using a LSM700 confocal microscope.

MT cosedimentation assay

For preparation of stabilized MT solution, purified tubulin dimers from porcine brain (Cytoskeleton Inc) were polymerized by incubating in PEM buffer (100 mM Pipes, pH6.8, 1 mM EGTA, 1 mM $MgCl_2$) with 1 mM GTP, 30% glycerol, and 10 μM taxol for 1 h at 37 °C and then centrifuged at 100,000*g* for 15 min at 27 °C. SaOS2 cells expressing KIF1C-Clover (WT or 4YF) with or without c-Src-Y527F-Myc were lysed with PEM buffer with 1% (v/v) TritonX-100, 50 mM NaF, 1 mM Na_3VO_4, 1 mM *p*-PMSF, 10 μg/ml leupeptin, and 10 μg/ml aprotinin and then centrifuged at 15,000 rpm for 15 min at 4 °C. The supernatant (whole cell lysate) was mixed with stabilized MT solution, incubated for 1 h at room temperature, and then centrifuged at 100,000*g* for 15 min at 27 °C. The pellet fractions were subjected to immunoblotting.

Quantification of fluorescence intensity and colocalization

Fluorescence images obtained with a LSM700 confocal microscope were processed for quantification using ImageJ. To measure fluorescence intensities of KIF1C-mCherry at the peripheral/nonperipheral cytoplasmic regions of cells, cytoplasmic regions within 10 μm distance from each cell vertex were defined as peripheral regions, while cytoplasmic regions at least 20 μm away from the cell vertex were defined as nonperipheral cytoplasmic regions. Intensity profiles were generated by drawing line segments within these regions, and the peak values at the peripheral cytoplasmic regions were divided by the mean values at the nonperipheral cytoplasmic regions. Colocalization between KIF1C-Clover and MTs was quantified using the Coloc2 plugin.

Statistical analysis

Statistical significance was analyzed using the one-way ANOVA followed by the Tukey test, the Kruskal-Wallis test followed by the Steel test, or Student's t test. $p < 0.05$ was considered statistically significant.

Data availability

All data are contained within the article.

Supporting information—This article contains supporting information.

Acknowledgments—We thank T. Itoh (Kobe Univ.) for Src-transformed NIH3T3 cells, M. Okada (Osaka Univ.) for pCX4bsr-c-Src-Myc and pCX4bleo-c-SrcY527F-Myc, and T. Oikawa (Hokkaido Univ.) for pEGFP-Tks5. We also thank I. Wada (Fukushima Medical Univ.) for critical feedback on imaging analysis and K. Hoshi (Fukushima Med. Univ.) for technical assistance.

Author contributions—T. S. investigation; T. S., K. I., and Y. O. methodology; T. S. validation; T. S. and M. E. formal analysis; T. S., M. N., K. I., Y. O., and Y. M. funding acquisition; T. S., M. N., and Y. M. writing–original draft; M. N., K. I., M. E., Y. O., and Y. M. writing–review and editing; M. N. and Y. M. conceptualization; M. N., M. E., and Y. M. supervision; M. N. and Y. M. project administration; K. I. and Y. O. resources.

Funding and additional information—This work was supported in part by grants from JST Moonshot R&D, Japan [JPMJMS2022 (Y. M.); JPMJMS2025-14 (Y. O.)], JST CREST, Japan [JPMJCR20E2 (Y. O.); JPMJCR20E5 (K. I.)], Japan Agency for Medical Research and Development (AMED), Japan [18gm5010001s0901 (Y. M.)] and MEXT, Japan/JSPS KAKENHI, Japan [21K20641 (T. S.); 20K07575 (M. N.); 19H05794 (Y. O.)].

Conflict of interest—The authors declare that they have no conflicts of interest with the contents of this article.

Abbreviations—The abbreviations used are: ECM, extracellular matrices; FBS, fetal bovine serum; FL, fluorescein; MMPs, matrix metalloproteinases; MTs, microtubules; PTPD1, Protein Tyrosine Phosphatase D1.

References

1. Valastyan, S., and Weinberg, R. A. (2011) Tumor metastasis: molecular insights and evolving paradigms. *Cell* **147**, 275–292
2. Eddy, R. J., Weidmann, M. D., Sharma, V. P., and Condeelis, J. S. (2017) Tumor cell invadopodia: invasive protrusions that orchestrate metastasis. *Trends Cell Biol.* **27**, 595–607
3. Linder, S. (2007) The matrix corroded: podosomes and invadopodia in extracellular matrix degradation. *Trends Cell Biol.* **17**, 107–117
4. Wisdom, K. M., Adebowale, K., Chang, J., Lee, J. Y., Nam, S., Desai, R., *et al.* (2018) Matrix mechanical plasticity regulates cancer cell migration through confining microenvironments. *Nat. Commun.* **9**, 4144
5. Beaty, B. T., Sharma, V. P., Bravo-Cordero, J. J., Simpson, M. A., Eddy, R. J., Koleske, A. J., *et al.* (2013) beta1 Integrin regulates Arg to promote invadopodial maturation and matrix degradation. *Mol. Biol. Cell* **24**, 1661–1675. S1661-1611
6. Bravo-Cordero, J. J., Oser, M., Chen, X., Eddy, R., Hodgson, L., and Condeelis, J. (2011) A novel spatiotemporal RhoC activation pathway locally regulates cofilin activity at invadopodia. *Curr. Biol.* **21**, 635–644
7. Magalhaes, M. A., Larson, D. R., Mader, C. C., Bravo-Cordero, J. J., Gil-Henn, H., Oser, M., *et al.* (2011) Cortactin phosphorylation regulates cell invasion through a pH-dependent pathway. *J. Cell Biol.* **195**, 903–920
8. Schoumacher, M., Goldman, R. D., Louvard, D., and Vignjevic, D. M. (2010) Actin, microtubules, and vimentin intermediate filaments cooperate for elongation of invadopodia. *J. Cell Biol.* **189**, 541–556
9. Oser, M., Yamaguchi, H., Mader, C. C., Bravo-Cordero, J. J., Arias, M., Chen, X., *et al.* (2009) Cortactin regulates cofilin and N-WASp activities to control the stages of invadopodium assembly and maturation. *J. Cell Biol.* **186**, 571–587
10. Ayala, I., Baldassarre, M., Giacchetti, G., Caldieri, G., Tete, S., Luini, A., *et al.* (2008) Multiple regulatory inputs converge on cortactin to control invadopodia biogenesis and extracellular matrix degradation. *J. Cell Sci.* **121**, 369–378
11. Sharma, V. P., Eddy, R., Entenberg, D., Kai, M., Gertler, F. B., and Condeelis, J. (2013) Tks5 and SHIP2 regulate invadopodium maturation, but not initiation, in breast carcinoma cells. *Curr. Biol.* **23**, 2079–2089
12. Crimaldi, L., Courtneidge, S. A., and Gimona, M. (2009) Tks5 recruits AFAP-110, p190RhoGAP, and cortactin for podosome formation. *Exp. Cell Res.* **315**, 2581–2592
13. Bowden, E. T., Onikoyi, E., Slack, R., Myoui, A., Yoneda, T., Yamada, K. M., *et al.* (2006) Co-localization of cortactin and phosphotyrosine identifies active invadopodia in human breast cancer cells. *Exp. Cell Res.* **312**, 1240–1253
14. Kelley, L. C., Ammer, A. G., Hayes, K. E., Martin, K. H., Machida, K., Jia, L., *et al.* (2010) Oncogenic Src requires a wild-type counterpart to regulate invadopodia maturation. *J. Cell Sci.* **123**, 3923–3932
15. Mader, C. C., Oser, M., Magalhaes, M. A., Bravo-Cordero, J. J., Condeelis, J., Koleske, A. J., *et al.* (2011) An EGFR-Src-Arg-cortactin pathway mediates functional maturation of invadopodia and breast cancer cell invasion. *Cancer Res.* **71**, 1730–1741
16. Enomoto, M., Hayakawa, S., Itsukushima, S., Ren, D. Y., Matsuo, M., Tamada, K., *et al.* (2009) Autonomous regulation of osteosarcoma cell invasiveness by Wnt5a/Ror2 signaling. *Oncogene* **28**, 3197–3208
17. Yamagata, K., Li, X., Ikegaki, S., Oneyama, C., Okada, M., Nishita, M., *et al.* (2012) Dissection of Wnt5a-Ror2 signaling leading to matrix metalloproteinase (MMP-13) expression. *J. Biol. Chem.* **287**, 1588–1599
18. Nishita, M., Park, S. Y., Nishio, T., Kamizaki, K., Wang, Z., Tamada, K., *et al.* (2017) Ror2 signaling regulates Golgi structure and transport through IFT20 for tumor invasiveness. *Sci. Rep.* **7**, 1
19. Kikuchi, K., and Takahashi, K. (2008) WAVE2- and microtubule-dependent formation of long protrusions and invasion of cancer cells cultured on three-dimensional extracellular matrices. *Cancer Sci.* **99**, 2252–2259
20. Kopp, P., Lammers, R., Aepfelbacher, M., Woehlke, G., Rudel, T., Machuy, N., *et al.* (2006) The kinesin KIF1C and microtubule plus ends regulate podosome dynamics in macrophages. *Mol. Biol. Cell* **17**, 2811–2823
21. Bhuwania, R., Castro-Castro, A., and Linder, S. (2014) Microtubule acetylation regulates dynamics of KIF1C-powered vesicles and contact of microtubule plus ends with podosomes. *Eur. J. Cell Biol.* **93**, 424–437
22. Efimova, N., Grimaldi, A., Bachmann, A., Frye, K., Zhu, X., Feoktistov, A., *et al.* (2014) Podosome-regulating kinesin KIF1C translocates to the cell periphery in a CLASP-dependent manner. *J. Cell Sci.* **127**, 5179–5188
23. van den Dries, K., Linder, S., Maridonneau-Parini, I., and Poincloux, R. (2019) Probing the mechanical landscape - new insights into podosome architecture and mechanics. *J. Cell Sci.* **132**, jcs236828
24. Murphy, D. A., and Courtneidge, S. A. (2011) The 'ins' and 'outs' of podosomes and invadopodia: characteristics, formation and function. *Nat. Rev. Mol. Cell Biol.* **12**, 413–426
25. Gimona, M., Buccione, R., Courtneidge, S. A., and Linder, S. (2008) Assembly and biological role of podosomes and invadopodia. *Curr. Opin. Cell Biol.* **20**, 235–241
26. Verhey, K. J., and Hammond, J. W. (2009) Traffic control: regulation of kinesin motors. *Nat. Rev. Mol. Cell Biol.* **10**, 765–777
27. Siddiqui, N., Zwetsloot, A. J., Bachmann, A., Roth, D., Hussain, H., Brandt, J., *et al.* (2019) PTPN21 and Hook3 relieve KIF1C autoinhibition and activate intracellular transport. *Nat. Commun.* **10**, 2693

28. Kendrick, A. A., Dickey, A. M., Redwine, W. B., Tran, P. T., Vaites, L. P., Dzieciatkowska, M., *et al.* (2019) Hook3 is a scaffold for the opposite-polarity microtubule-based motors cytoplasmic dynein-1 and KIF1C. *J. Cell Biol.* **218**, 2982–3001
29. Theisen, U., Straube, E., and Straube, A. (2012) Directional persistence of migrating cells requires Kif1C-mediated stabilization of trailing adhesions. *Dev. Cell* **23**, 1153–1166
30. Dorner, C., Ciossek, T., Muller, S., Moller, P. H., Ullrich, A., and Lammers, R. (1998) Characterization of KIF1C, a new kinesin-like protein involved in vesicle transport from the Golgi apparatus to the endoplasmic reticulum. *J. Biol. Chem.* **273**, 20267–20275
31. Beaty, B. T., and Condeelis, J. (2014) Digging a little deeper: the stages of invadopodium formation and maturation. *Eur. J. Cell Biol.* **93**, 438–444
32. Blom, N., Sicheritz-Ponten, T., Gupta, R., Gammeltoft, S., and Brunak, S. (2004) Prediction of post-translational glycosylation and phosphorylation of proteins from the amino acid sequence. *Proteomics* **4**, 1633–1649
33. Farkhondeh, A., Niwa, S., Takei, Y., and Hirokawa, N. (2015) Characterizing KIF16B in neurons reveals a novel intramolecular "stalk inhibition" mechanism that regulates its capacity to potentiate the selective somatodendritic localization of early endosomes. *J. Neurosci.* **35**, 5067–5086
34. Hammond, J. W., Blasius, T. L., Soppina, V., Cai, D., and Verhey, K. J. (2010) Autoinhibition of the kinesin-2 motor KIF17 via dual intramolecular mechanisms. *J. Cell Biol.* **189**, 1013–1025
35. Hammond, J. W., Cai, D., Blasius, T. L., Li, Z., Jiang, Y., Jih, G. T., *et al.* (2009) Mammalian kinesin-3 motors are dimeric *in vivo* and move by processive motility upon release of autoinhibition. *PLoS Biol.* **7**, e72
36. Ridley, A. J. (2011) Life at the leading edge. *Cell* **145**, 1012–1022
37. Moller, N. P., Moller, K. B., Lammers, R., Kharitonenkov, A., Sures, I., and Ullrich, A. (1994) Src kinase associates with a member of a distinct subfamily of protein-tyrosine phosphatases containing an ezrin-like domain. *Proc. Natl. Acad. Sci. U. S. A.* **91**, 7477–7481
38. Cardone, L., Carlucci, A., Affaitati, A., Livigni, A., DeCristofaro, T., Garbi, C., *et al.* (2004) Mitochondrial AKAP121 binds and targets protein tyrosine phosphatase D1, a novel positive regulator of src signaling. *Mol. Cell. Biol.* **24**, 4613–4626
39. Akagi, T., Sasai, K., and Hanafusa, H. (2003) Refractory nature of normal human diploid fibroblasts with respect to oncogene-mediated transformation. *Proc. Natl. Acad. Sci. U. S. A.* **100**, 13567–13572
40. Oikawa, T., Oyama, M., Kozuka-Hata, H., Uehara, S., Udagawa, N., Saya, H., *et al.* (2012) Tks5-dependent formation of circumferential podosomes/invadopodia mediates cell-cell fusion. *J. Cell Biol.* **197**, 553–568
41. Oikawa, T., Itoh, T., and Takenawa, T. (2008) Sequential signals toward podosome formation in NIH-src cells. *J. Cell Biol.* **182**, 157–169
42. Nishita, M., Yoo, S. K., Nomachi, A., Kani, S., Sougawa, N., Ohta, Y., *et al.* (2006) Filopodia formation mediated by receptor tyrosine kinase Ror2 is required for Wnt5a-induced cell migration. *J. Cell Biol.* **175**, 555–562